Egypt. J. Chem. **58**, No. 6, pp. 681-697 (2015)

Interaction Characteristics Governing the Synthesis of Magnetite Nanoparticls-conjugated Poly (amido amine) Dendrimer-based Rice Straw Ash

S. A. Hassan[#], A. S. Darwish, Nour E. A. Abed-Elsatar, Heba A. Gobara[*] and Safaa A. Rushdy

Department of Chemistry, Faculty of Science, Ain Shams University, Abbassia 11566, Cairo and [*]Catalysis Department, Refining Division, Egyptian Petroleum Research Institute, Nasr City, 11727, Cairo, Egypt.

THE PARENT magnetite NPs@ poly (amido amine) dendrimer (PAMAM) composite was synthesized through one pot reaction pathway. Different hybrid nanocomposites of magnetite (M NPs) of different concentrations ($1*10^{-3}$ and $3*10^{-3}$ M) conjugated in situ with dendrimer (PAMAM)@ rice straw ash (RSA) filler were also synthesized. The finished as-synthesized nanocomposites were characterized adopting the XRD, BET, FTIR, DLS, SEM and TEM techniques. The results revealed that magnetite species are conjugated with dendrimer branches through N-O-Fe linkages. In hybrid M NPs@PAMAM@RSA nanocomposites, the presence of RSA binder seemed to encourage the intimate interactions with dendrimer branches through Si-OH of the ash and Fe-O-N conjugations; carbon prevailing in composite space appeared almost filling the dendrimer cavities. The MNPs-anchored-dendrimer existed as dispersed cubic nanocrystallites embedded in the dendrimer matrix.

Keywords: Poly (amido amine) dendrimer, Magnetite nanoparticle, Rice straw ash and Hybrid nanocomposites.

According to the infinite network theory of Flory, the presence of three dimensional dendritic branching concepts produced four novel types of architectural polymers called dendritic polymers. These classes of dendritic polymers are classified into four subdivided species: (a) random hyperbranched, (b) dendrigrafts, (c) dendrons, and (d) dendrimers. Dendrimers are monodispersed, hyper-branched, polyfunctional polymers encompassing initiator core, interior layers of diverse generations and exterior layers of terminal function groups[(1)]. Dendrimers are also susceptible to exist in various architectural forms, *e.g.* bow-tied, ball-shaped, bola-form, multi-branched, cauliflower, … etc, like structures. There are few examples of dendritic architectures in the nanoscale such as the glycogen and amylopectin hyperbranched structures that are used for energy storage. The most popular type of dendrimers is the poly (amido-amine) dendrimers (PAMAM) made by Tomalia *et al.* (1985)[(2)]. Nowadays, more attention has been paid for exploring innovative structures of dendrimers and using them as filters in nanocomposite technology.

[#]Corresponding author, e-mail:salahabdo@yahoo.com

On the other hand rice straw is one of the most agriculture waste produced through milling of rice,burning of which represents a serious problem in rice-producing countries. Rice straw consists of cellulose and amorphous silica as 20 % ash, 38 % cellulose, 22 % lignin, 18 % pentose, and about 2 % of other organic components [14]. When the rice straw is burned it gives 10-14 % by its weight ash containing >90 % of crystalline silica [3] and small amount of other elements. Ashes are used in various applications depending on specified characteristics, such as ceramic industry which requires chemical purity and reactivity for cement and concrete, metal catalysts requiring high surface area and porosity as well as synthesis of porous carbon, silicon carbide and zeolites. Ashes are also used as additives, fillers, oil adsorbents, … etc [4].

Dendrimes seem to be highly candidated as beneficial support for metal, metal oxide and metal complexes due to their ability to stabilize the metallic particles enhancing the activity and selectivity of metal nanoparticles toward various catalytic processes.

Magnetite (Fe_3O_4) is the common oxide of magnetic iron, which possesses a cubic inverse spinal structure. Synthetic magnetite nanoparticles have wide applications due to their unique magnetic properties associated with uniform distribution. Magnetite NPs are used also in catalysis as well as biomedical applications such as enzyme immobilization, anticancer and magnetic resonance[5].

The present study was undertaken to follow up the interaction characteristics governing the synthesis events of a new developed type of magnetite (M) NPs @ poly amidoamine (PAMAM) dendrimer@ rice straw ash (RSA) nanocomposite to be standardized for further applications of industrial and environmental impacts.

Experimental

Synthesis of PAMAM dendrimers

Synthesis of (G=2) star PAMAM-$(NH_2)_{16}$

To a vigorously stirred solution of ethylenediamine (476.37 g, 524.06 ml, 7939.55 mmol) in methanol, a solution of star PAMAM $(COOMe)_{16}$ (G=1.5)(50 g, 17.83 mmol) was added under nitrogen at 0^o C over a period of 2 hr [6]. The solution was allowed to warm to room temperature and stirred for further 96 hr. The product was purified by using azeotropic mixture of toluene/methanol = 9:1 under vacuum at 40^o C, giving a deep yellow oily product (star PAMAM-$NH_2)_{16}$[2].

Preparation of rice straw ash (RSA)

The collected rice straw (from Kafr El-Zayat region) was thoroughly washed with distilled water to remove adhering soil and clay and sieved to 250-500 µm. The ash was obtained through controlled burning in a temperature-programmed oven at 600° C for 4hr.

Synthesis of pure magnetite nanoparticles

In 125 ml Erlenmeyer flask, (2 g) of ferrous sulfate $FeSO_4.7H_2O$ (99%-Aldrich) and (5 g) ferric chloride $FeCl_3.6H_2O$ (99%-Aldrich) were dissolved in

25 ml distilled H_2O (PAMAM@RSA). Thereafter, 0.85 ml of conc.HCl was added to this mixture under vigorous mechanical stirring. A solution of NaOH (2M, 250 ml H_2O) was added dropwise till a black precipitate was formed (pH ~ 14). The produced NPs were collected by means of a magnet. □

Synthesis of the mother (M NPs@PAMAM)nanocomposite

In a 250 ml flask, (0.00834 gm) of ferrous sulphate $FeSO_4.7H_2O$, (0.0216 g) of $FeCl_3.6H_2O$ and a stoichiometric amount of PAMAM dendrimer (G=2, 1 g), in a molar ratio of precursor/dendrimer = 1: 20, were dissolved in 25 ml of distilled water, then 0.004 ml of conc HCl was added. A solution of NaOH (1M, 4 g, 50 ml H_2O) was added dropwise with stirring till a black precipitate was formed (pH ~ 14). The produced NPs were collected by a magnet.

Preparation of magnetite-rice straw ash-PAMAM dendrimernanocomposite

A 6.5 g of dry rice straw ash (RSA) was slowly added to PAMAM dendrimer (G=2, 1g) dissolved in 10 ml of isopropanol. 0.00139 g of ferrous sulfate, $FeSO_4.7H_2O$, and 50.0360 g of ferric chloride, $FeCl_3.6H_2O$, in 10 ml of 0.2 M HCl were mixed with the PAMAM@RSA composite with boiling under vigorous stirring. NaOH (2M, 250 ml H_2O) was added dropwise till (pH ~14). The mixture was stirred at room temperature for 24 hr, after which it was left to stand then decanted, filtered and washed several times with H_2O and then with acetone.

Characterization techniques

The as-synthesized nanocomposites were characterized via FT-IR spectra, recorded on a JASCO spectrophotometer model FT/IR-420, using KBr disc technique in the wave number range of 4000 to 200 cm^{-1}. Proton nuclear magnetic resonance (^{1}H-NMR) spectra were measured on a Varian Mercury 300 (300 MHz) instrument.The crystalline structure and the different phases were investigated via X-ray diffraction analysis (XRD) using Shimadzu XD-1 diffractometer. The phase identification was made according to the Joint Committee on Powder Diffraction Standards (JCPDS). The crystallite size, $D\text{-}_{XRD}$ was calculated according to Scherer equation [7].

$$D_{XRD} = \frac{K\lambda}{\beta \cos(\theta)}$$

where k is the Sherrer constant (0.89), λ is the wavelength of the X-ray radiation (0.15418 nm for Cu Kα), β is the full width at half maximum (FWHM) of the diffraction peak measured at 2θ, and θ is the diffraction angle. The textural properties were followed up using the N_2 adsorption-desorption isotherms measured at -196°C using NOVA-2000 gas sorption analyzer. The morphology of the synthesized nanocomposites was investigated via JSM 7500FA- High Resolution Cold Field Emission SEM and by transmission electron microscopy (TEM) via JEM 1011. The size and electrokinetic potential were measured using a Nano Series Zeta Sizer, Malvern; Worcestershire, UK. The particle size distribution and hydrodynamic diameter of different nanocomposites were evaluated through Dynamic Light Scattering (DLS). Each sample (0.5 mg/ml) was suspended in deionized water and ultrasound-irradiated for 5 min. The suspension

was then kept at room temperaturefor 24 hr under vigorous stirring. The pH was then adjusted at 7.4 and zeta potential values were evaluated at 30°C. All measurements were performed for five replicates and averaged to get the final value.

Results and Discussion

Physicochemical characteristics of PAMAM dendrimer

H^1 NMR and C^{13} NMR measurement of PAMAM dendrimers

In this study, the starting PAMAM dendrimer (G=1.5) was formed by addition of methyl acrylate to G=1, to be terminated by 16 acrylate groups as indicated by C^{13} NMR spectrum shown in Fig.1. The analysis reveals the following: C^{13} NMR spectrum (DMSO) δ_C: 49.573 (a), 49.115 (b), 32.419 (c), 37.833 (d), 51.251 (e), 172.650 (x), 172.764 (x_1), 172.829 (y), 52.016 (z).

Also, the elemental analysis data of PAMAM dendrimer (G=1.5) and that one of (G=2) are summarized in Table 1.

TABLE 1. Elemental analysis data of PAMAM dendrimer (G=1.5) and that one of (G=2).

Generation	C%		H%		N%	
	Found	Calc	Found	Calc	Found	Calc
G=1.5 $C_{126}H_{226}N_{26}O_{44}$	54.1	53.9	8.9	8.1	14	12.9
G=2 $C_{142}H_{288}N_{58}O_{28}$	48.5	52.4	9.3	8.89	22.9	24.9

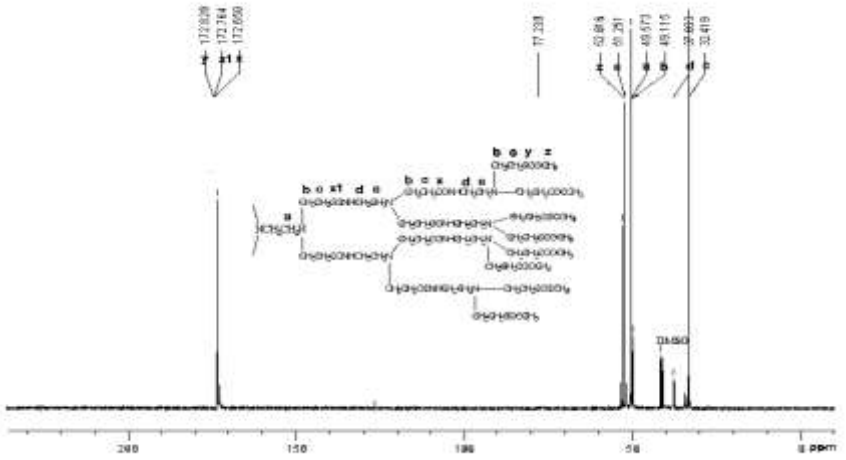

Fig. 1. C^{13}NMR dendri-PAMAM $(COOCH_3)_{16}$.

FTIR investigation

FT-IR spectra of the parent PAMAM (poly amido amine dendrimer, (G=2) as well as the conjugated magnetite-dendrimer (M NPs@PAMAM composite) are depicted in Fig. 2. For PAMAM (G=2) (Fig. 2, a), the peak at 3270 cm^{-1} is attributed to the bending vibration of primary amine ($-NH_2$) and that are at 3059 cm^{-1} is due to secondary amine (-NH). Also, the two sharp peaks at 1683 and 1584 cm^{-1} are due to (-CO-NH-) groups. In addition, the weak peak at 1200 cm^{-1} is referred to (C-C) bending and those the peaks at 1471 and 2830 cm^{-1} are related to ($-CH_2$) groups. However, the characteristic peaks of molecular water are assigned at 3270 cm^{-1} and 3059 cm^{-1}. For PAMAM dendrimer-conjugated magnetite nanoparticles (M NPs@PAMAM), beside the characteristic peaks of PAMAM two new absorption peaks appeared. The first one at 597 cm^{-1} is attributable to Fe-O of magnetite (intrinsic stretching vibration at tetrahedral site Fe_{teta}-O) and the second one at 1044 $cm^{-1}$of (N-O), which may suggest the overall formation of (N-O-Fe) linkages [8]. It is clear that these two peaks (3059 cm^{-1} of primary amine and 3270 cm^{-1} of secondary amine) are subject of masking (overlapping) with a somewhat shifted broad peak maximized at 3442 cm^{-1} assigned most probably to the molecular water in magnetite moieties [9].

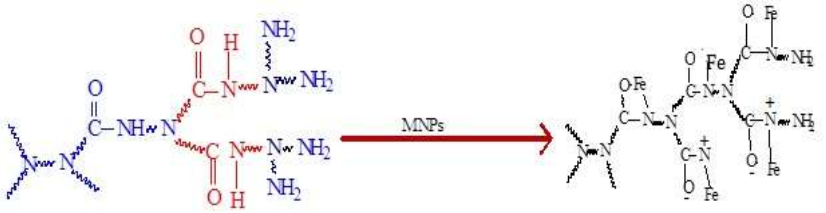

Scheme 1.Proposed mechanism of the formation of (M NPs@PAMAM).

The FT-IR spectra of RSA and ($3*10^{-3}$M) M NPs @ PAMAM @ RS Ananocomposite are represented in Fig. 2(b). For neat RSA the broad peak at 480 – 460 cm^{-1} is assigned to Si-O-Si bending characterizing the amorphous silica content. The peak at 1030 cm^{-1} is referred to SiO_2 lattice vibration and that one at 3867 cm^{-1} is related to (ν O-H) vibration. The weak peaks in the range of 1340-1490 cm^{-1} seem to be due to $–CH_2-$, CH_3 and COOH vibrations arisen from carbon-content of the ash. For the M NPs@PAMAM@RSA system, the peak at 465 cm^{-1} belongs to the bending vibration of [ν (O-Si-O)] of RSA. Also, the peaks at 1074 cm^{-1} and 790 cm^{-1} are assigned to [ν (Si-O-Si)] stretching vibration modes of RSA; becoming more pronounced than the corresponding ones in the original sample of RSA. The characteristic peak shifted at 618 cm^{-1} eviedently belongs to magnetite (Fe-O). It is to be mentioned that the peak at 1638 cm^{-1} in the nanocomposite is assigned to the -CO-NH- groups of PAMAM, while that new one at 1738 cm^{-1} may refer to formation of Fe-O-N bond with the dendrimer (Scheme 1). In this regard, the broad peak at 3565 cm^{-1} is corresponding to water content in both magnetite and RSA in M NPs@PAMAM@ RSA composite.

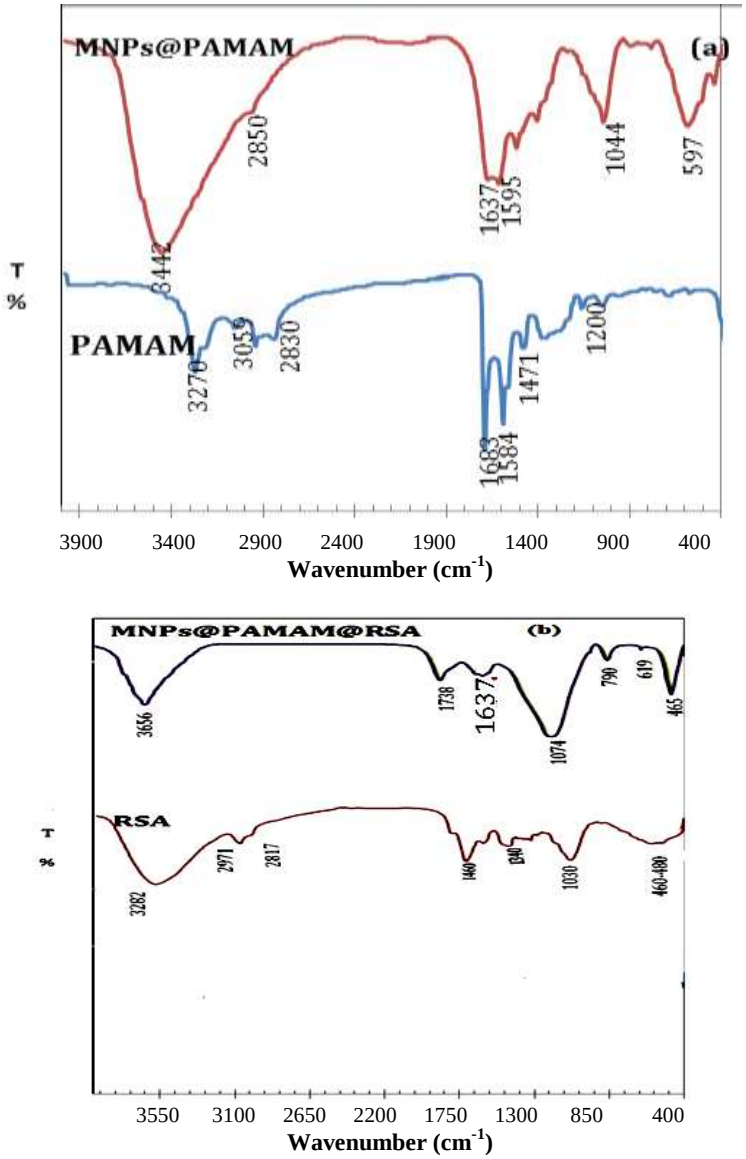

Fig. 2. FT-IR spectra of (a) PAMAM and M NPs @PAMAM and (b) RSA and M NPs ($3*10^{-3}$ M) M NPs@PAMAM@RSA.

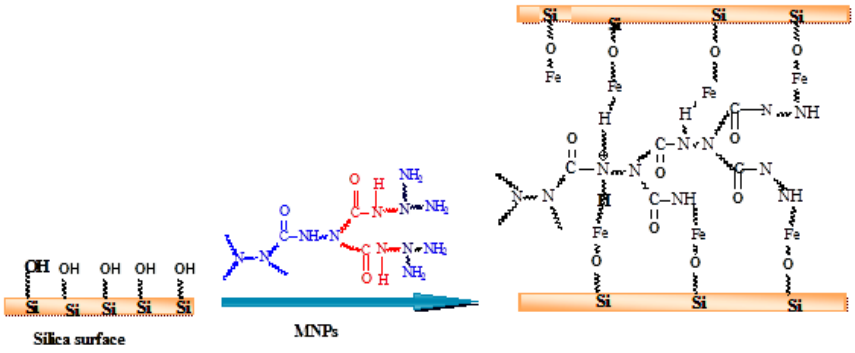

Scheme 2.Proposed mechanism of the formation of (M NPs@PAMAM@RSA).

XRD analysis

The XRD pattern illustrated in Fig. 3 (a) for pure magnetite nanoparticles shows characteristic peaks at 2θ=18.4°,29.4°, 35.1°, 42.5° ,52.8°, 55.5°, and 75.6° corresponding to (111), (220), (311),(400), (422), (511), and (533) Miller indices with lattice spacings (d): 4.8, 3.0, 2.5, 2.1, 1.37, 1.65 and 1.25 nm, respectively. The position and relative intensity of the peaks in the obtained pattern agree well with those of magnetite (JCPDS card No 89-0691). This indicates that magnetite in this study has an inverse spinel structure with a face centered cubic form[10]. In addition, all the characteristic peaks typical of γ-Fe_2O_3 and α-Fe_2O_3 are neglected in the present study to simplify the comparison of different synthesis parameters.

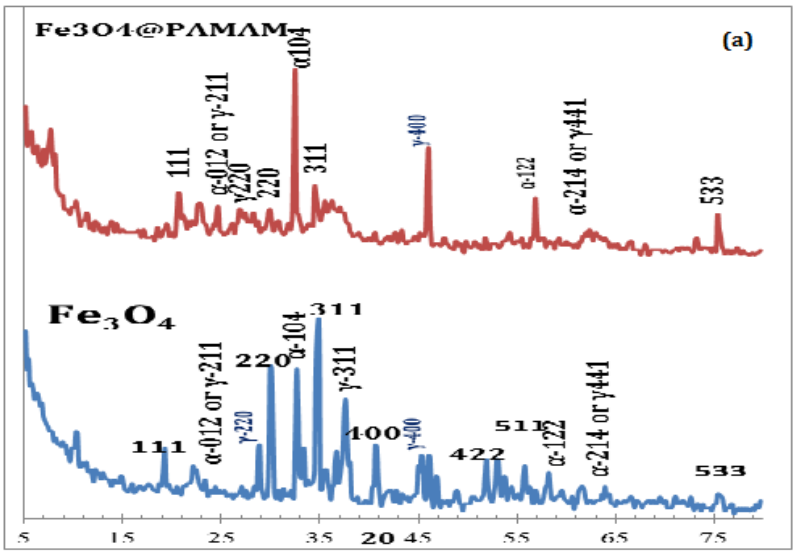

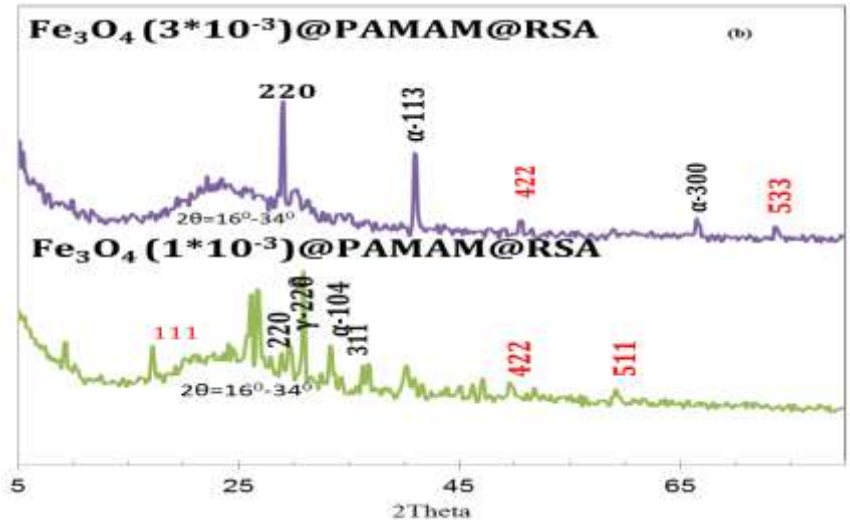

Fig. 3. XRD patterns of (a) pure M NPs and parent M NPs @PAMAM nanocomposite and (b) M NPs (1*10^{-3}M and 1*10^{-3}M) @PAMAM@RSA.

The mean crystallite size of pure magnetite (D_{XRD}) determined by Scherrer equation (Table 2) was found to be 35.1, 42.8, 39.1, 37, 34.2, 39.1 and 23.1 nm corresponding to (111), (220), (311), (400), (422),(511) and (533) of magnetite facets, respectively. For the comparative purposes, the average particle sizes calculated for M NPs at 2θ=35.1^{o} (311) and 55.5^{o} (511) being equal (viz., 39.1 nm) will be taken as reference for the other composite systems.

TABLE 2. XRD data and particle size calculated from Scherrer equation for M NPs and the mother M NPs@PAMAMnanocomposite.

System	2θ	Fe_3O_4 (h k l)	Particle size (nm)	d-Spacing
Fe_3O_4 (M NPs)	18.4	111	35.1	4.8
	29.4	220	42.8	3.0
	35.1	311	39.1	2.5
	42.5	400	37	2.1
	52.8	422	34.2	1.7
	55.5	511	39.1	1.3
	75.6	533	23.1	1.2
Fe_3O_4@PAMAM	18.4	111	34.2	4.4
	29.4	220	28.5	3.0
	35.1	311	27.7	2.6
	52.8	422	Disappeared	
	55.5	511	Disappeared	
	75.4	533	91.31.2	

By comparing the patterns of magnetite in the mother M NPs@PAMAM composite with that of pure magnetite reference sample, it can be seen clearly that the average crystallite sizes of M NPs have been reduced in the synthesized composite (M NPs@ PAMAM), viz., with the following extents: 0.9 nm at $2\theta=18.4^{o}$ (111), 14.3 nm at $2\theta=29.4^{o}$ (220) and 16.4 nm at $2\theta=35.1^{o}$ (311). In view of disappearance of M NPs peak at $2\theta=55.5^{o}$(511) in the parent composite, one can conclude that magnetite has been interacted with PAMAM, *i.e.* most probably through bulk CO-NH linkages in cavities. The M NPs are incorporated in the PAMAM matrix as encapsulated species of markedly reduced average sizes.

The XRD diffraction patterns of M NPs@PAMAM@RSA system with two different ratios of magnetite ($1*10^{-3}$ and $3*10^{-3}$) are illustrated in Fig. 3. All samples show a broad hump in the 2θ ranging from 16^{o} to 34^{o} related most probably to the amorphous silica phase in RSA. For M NPs@PAMAM@RSA ($1*10^{-3}$) system, in addition to amorphous silica phase, the peaks at $2\theta=18.1^{o}$, 29.6^{o}, 35.1, 52.3^{o} and 75.6^{o} corresponding (111), (220), (311), (422) and (533) Miller indices of magnetiteare observed. The corresponding reduction extents in average crystallite sizes of Fe_3O_4 are 18.0, 16.5, 25.8 and 18.7 nm at corresponding (111), (220), (311) and (422), respectively. The peak at 75.6^{o} (533) disappeared indicating the evident interaction of M NPs during its conjugation with the RSA-PAMAM network.

For the M NPs@PAMAM@RSA ($3*10^{-3}$M) system, the same reduction trend in average crystallite sizes was obtained at (422) and (511), together with disappearance of the peak at 35.1^{o} (311).

In conclusion, it is noticed that the particle size of pure magnetite is decreased due to its encapsulation in PAMAM dendrimermatrix and continues to decrease through anchorage to RSA.

TABLE 3. XRD data and particle size calculated from Scherrer equation for M NPs@PAMAM@RSA ($1*10^{-3}$M) and the M NPs@PAMAM@RSA ($3*10^{-3}$M)nanocomposites.

System	2θ	Fe3O4 (h k l)	Particle size (nm)	d-Spacing
Fe3O4@PAMAM@RSA (1*10-3M)	18.1	111	17.1	4.9
	29.6	220	26.3	3
	35.1	311	13.3	1.2
	52.3	422	15.5	1.7
	75.6	533	Disappeared	
Fe3O4@PAMAM@RSA (3*10-3M)	29.6	220	11.2	1.7
	35.1	311	Disappeared	
	52.5	422	7.7	1.6
	55.2	511	53.6	1.2
	75.6	533		

Surface study

Inspection of Table 4 indicates that M NPs@PAMAM exhibits noticeably small surface area (7.8 m^2/g). This may be linked with the anchorage of M NPs to the -NH & -C=O sites of PAMAM dendrimermain core [11]. By adding RSA (of S_{BET}=14.5 m_2/g) [14], the produced composite M NPs @PAMAM@RSA shows some increase in surface area, viz, 9.4 m^2/g, arising from both the pore system of RSA and cavity structure of PAMAM.

TABLE 4. Surface area parameters of M NPs@PAMAM and ($1*10^{-3}$ M and $3*10^{-3}$ M) M NPs@PAMAM@RSA nanocomposites.

Adsorb	C_{BET}	Vm Cm^3/g	S_{BET} (m^2/g)	Total pore volume (V_p) (ml/g)	Average pore radius (r_p)(Å)	Most abundance approximate pore radius ($r_{m.abund}$)(nm)
M NPs@PAMAM	11.3	1.7	7.8	0.0280	74.1	3.7
M NPs($1*10^3$)@PAMAM@RSA	8.9	2.1	9.4	0.0184	38.9	1.7
M NPs ($3*10^3$)@PAMAM@RSA	5.6	1.3	5.8	0.0155	54.5	1.6

To confirm the overall pore system of the finished composite, the pore parameters of the components can be compared. The pore system of M NPs @PAMAM represents dendrimer cavities of average pore radius 7.4 nm (wide pores), with total pore volume of 0.028 cm^3/g, while the pore system of RSA represents narrower mesopores of 1.4 nm with larger pore depth of 0.074 cm^3/g, reflecting the mixed pore structure of the ash.

For M NPs@PAMAM@RSA, the average pore radius is 3.9 nm, *i.e.*, with a considerable decrease in the cavities parameters (r_p from 7.4 nm to 3.9 nm and v_p from 0.028 cm^3/g to 0.018 cm^3/g) linked with some filling by RSA particles. On the other hand, the increase in RSA pore radius (from 1.4 nm to 3.9 nm) confirms the coverage and filling process(*cf.*, the change of v_p from 0.074 to 0.018). The obtained results are well documented by the pore size distribution (PSD) curves in Fig. 4.

Dynamic light scattering (DLS) study for MNPs @ PAMAM

Zeta potential (ζ) study

The zeta potential data measured at pH 4 and 9 are summarized in Table 5, while the hydrodynamic particle size distributions are illustrated in Fig.5. For the mother M NPs @PAMAM, the zeta potential (ζ) measured in acidic medium (pH=4) is (+4.09 mV), referring to the retained positively charged NH-groups in the dendrimer core, overcoming in the same time the negative charges of magnetite nanoparticles (M NPs). In the basic medium, pH=9, ζ is highly negative (-25.7 mV), *i.e.*, referring to the magnetite particulates exposed on the dendrimer surface.

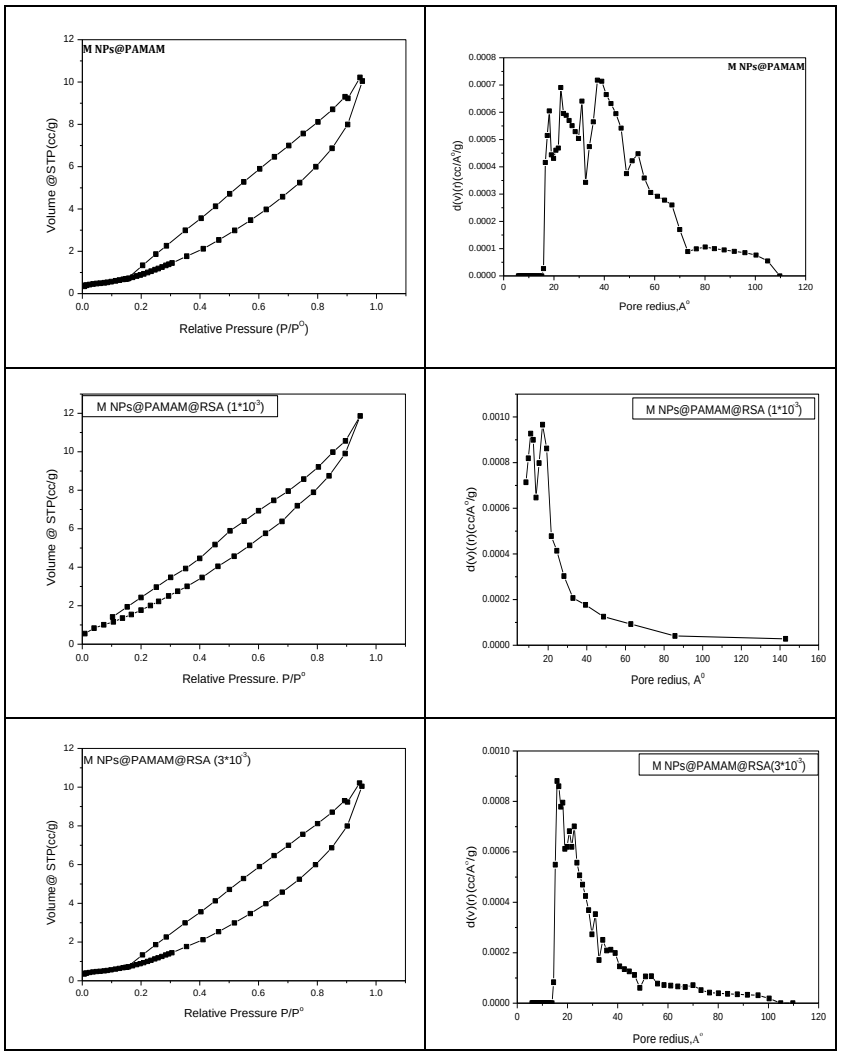

Fig. 4. N_2-Adsortion-desorption isotherms and particle size distribution (nm) of parent M NPs @PAMAM nanocomposite and M NPs ($1*10^{-3}$M and $1*10^{-3}$M) @PAMAM@RSA. M NPs@PAMAM.

For the ($1*10^{-3}$ M) M NPs @PAMAM@RSA composite, the ζ value is -12.5 mV (at pH=4), *i.e.*, an apparent decrease in ζ of the mother M NPs @PAMAM is evident. This may confirm the suggested interaction profile of RSA (through Si-O site) with the terminal groups amines of the dendrimer branches, rather

than with M NPs sited at the core, leaving some negatively charged magnetite nanoparticlesbe exposed.

TABLE 5. DLS and zeta potential parameters of M NPs@PAMAM and ($1*10^{-3}$ M and $3*10^{-3}$ M) M NPs@PAMAM@RSAnanocomposites.

Composites	Zeta potential (ζ) (mV)		Conductivity ($\mu S/cm^{-1}$)	
	pH=4	pH=9	pH=4	pH=9
M NPs@PAMAM	4.09	-25.7	4.71	6.99
M NPs(1*103M)@PAMAM@RSA	-12.5	-28.7	4.75	6.73
M NPs(3*103M)@PAMAM@RSA	-5.52	-25.5	4.51	6.86

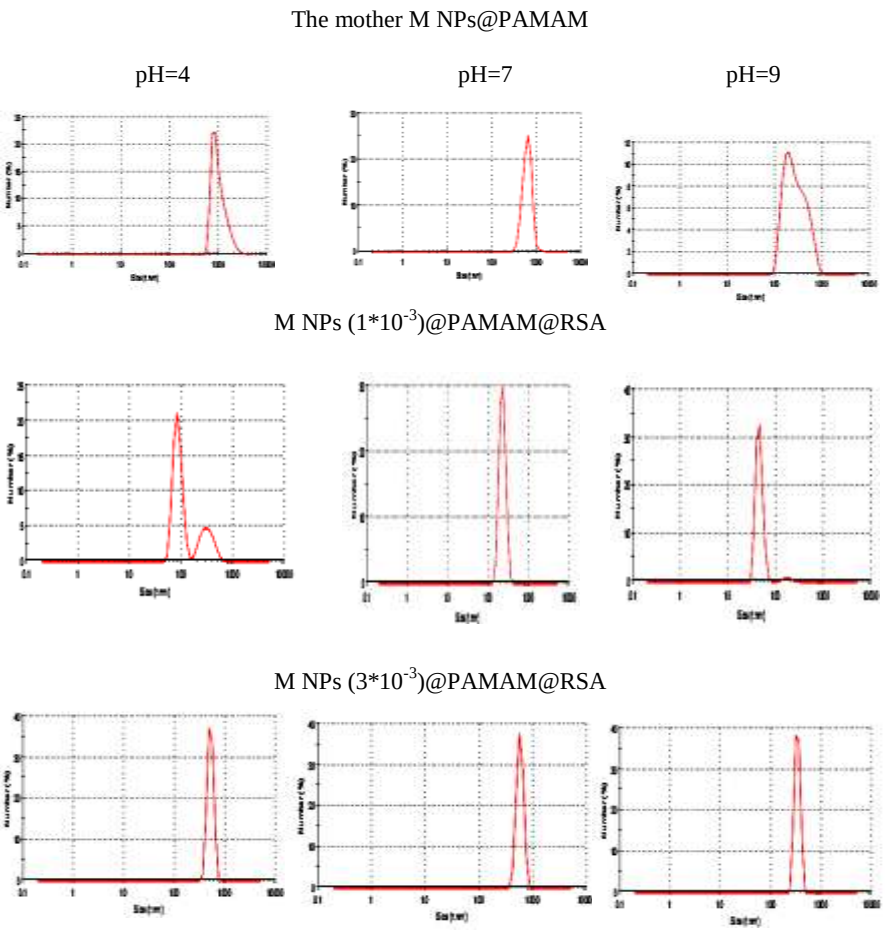

Fig. 5. Hydrodynamic particle size distribution profiles of different nanocomposite.

On the contrary, when the M NPs concentration increases to $3*10^{-3}$ M (at pH=4), the RSA seems to interact not only with the branch amine of dendrimer but also with the excess M NPs exposed on the dendrimer surface. Thus, the charge tends to be positive (ζ+5.52) approaching that of the mother M NPs@PAMAM. Again at pH=9, the increase in basicity may be reflected in the more negative charges (or ζ- 28.7 and -25.2)following the same mechanism described for the different concentrations. Such increase in the basicity may be linked with the expansion of the electric double layer (high negative charge density).

Particle size distribution (PSD) study

For the hydrodynamic particle size distributions represented in Fig. 5, it is clear that the average particle size of this M NPs@PAMAM is decreased gradually and markedly from 1032 nm to 300 nm by increasing the pH value of the solution from 0.4 to 0.9; the colloidal M NPs tending to be more stable especially in alkaline medium. Such behavior is in compliance with rising of zeta-potential values (more -ve), *i.e.*, expressing the repulsive forces between M NPs@PAMAM colloidal particles.

For the ($1*10^{-3}$ M) M NPs@PAMAM@RSA composite, the increase of solution pH is accompanied by a decrease in average particle size achieving 45 nm (at pH=9), linked probably with more pronounced repulsion forces and ζ values. On the other hand, the presence of RSA as co-binding component seems to encourage the intimate interaction with the dendrimer in favor of the M NPs. As an evidence for this behavior, at pH=4, the bimodal particle size distribution may point to the intimate interaction of RSA with the dendrimer. By increasing the concentration of M NPs to $3*10^{-3}$M, the same trend of particle size reduction is observed (from 512 nm to 332 nm) by increasing the pH value up to 9.

TEM study

The morphology and dispersion of M NPs in mother M NPs@PAMAM nanocomposite are represented in Fig. 6 (a). The dendrimer branches are seen as separate stacks, distributed in some organized shape. The magnetite nanoparticles are located mainly on the dendrimer branches and in their cavities in an uneven dispersion profile with average particle sizes 4, 6 and 10 nm.

For ($1*10^{-3}$M)@PAMAM@RSA (Fig. 6, b), it is evident that the magnetite cubic nanocrystallites are dispersed mainly on dendrimer network having average sizes ranged between 35-52 nm, covering also most of the cavities.

For the higher concentration ($3*10^{-3}$ M)@PAMAM@RSA(Fig. 6, c and d)), the images show the embedded M NPs in some cubic structure together with the major dispersion of small dots (image c), clearly linked through the intimate interaction between RSA and PAMAM matrix. This type of interaction is more pronounced in image (d) where the whole structure of the nanocomposite is associated with anchorage of well dispersed M NPs in even distribution between the RSA and PAMAM phases.

SEM study

The SEM images of different PAMAM-base composites under study are shown in Fig. 7. The images (a and b) of mother M NPs@PAMAM, indicate the even distribution of M NPs over PAMAM blocks. Some of them are introduced into the dendrimer cavities as accumulated bright pellets. For ($3*10^{-3}$ M)@PAMAM@RSA, the images (c and d) reveal the whole network of PAMAM, majoring as a field, with organized fine granules and well attached sets intimately interacted with RSA sticks. The M NPs are distributed evenly in this interaction phases (c). The protrusions of PAMAM, intimately interacted with covering RSA sticks and with magnetite needles and dots, are well documented in the highly magnified image (d).

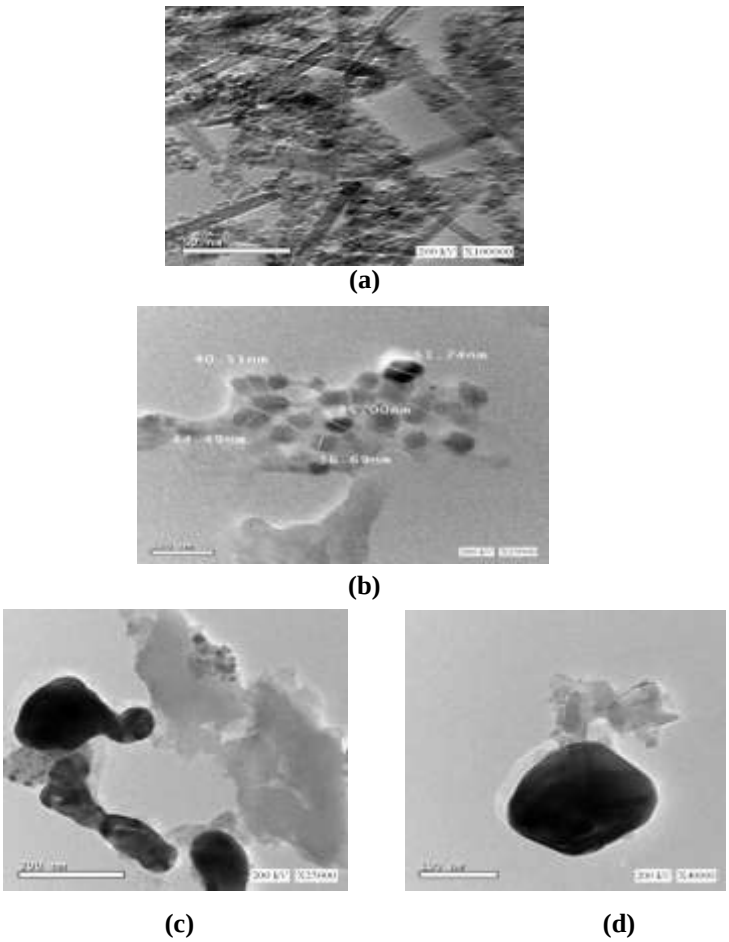

(a) **(b)** **(c)** **(d)**

Fig. 6 (a). TEM images of M NPs@PAMAMnanocomposite, (b) M NPs ($1*10^{-3}$ M) @PAMAM@ RSA nanocomposite and (c, d) M NPs ($3*10^{-3}$ M) @PAMAM@ RSA nanocomposite.

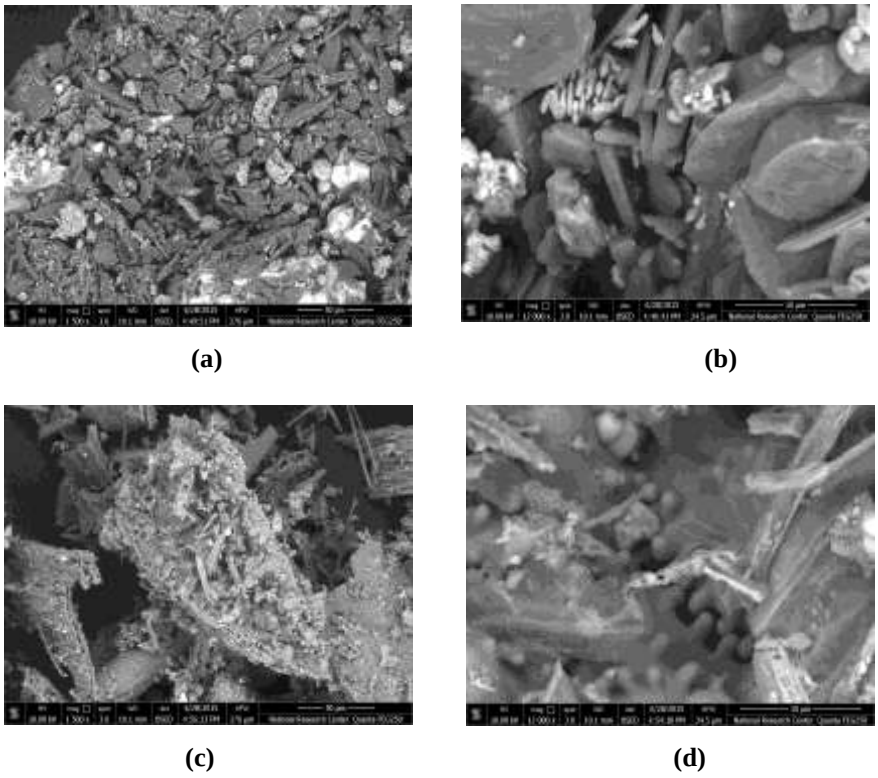

(a) **(b)**

(c) **(d)**

Fig. 7. SEM images of M NPs@ PAMAM (a,b) and M NPs@PAMAM@RSA (c,d).

Conclusion

In the present study, magnetite nanoparticles (M NPs) were immobilized into poly (amido amine) (PAMAM) dendrimer in the mother nanocomposite(M NPs @ PAMAM). The M NPs were conjugated with dendrimer matrix through formation of N-O-Fe linkages. This was accompanied with a reduction inmagnetite average particle size from 39.1 nm (311) in pure M NPs to 27.7 nm (311) in M NPs @PAMAM. The incorporated M NPs seemed to be embedded in dendrimer matrix, mainly on coreand cavities, in some uneven distribution.

For the hybrid M NPs@PAMAM@RSA, M NPs were conjugated from side with PAMAM through CO-NH linkages and through Si-O- linkages of the RSA. The presence of RSA encouraged intimate interaction with dendrimer branches, through Si-OH of the ash and Fe-O-N conjugations; carbon prevailing in composite space appeared almost filling the dendrimer cavities. The M NPs-anchored-dendrimer existed as dispersed cubic nanocrystallites embedded in the dendrimer matrix.

References

1. **Tomalia, D.A.,** The dendritic state. *Maerials Today*, **34** (2005).

2. **Tomalia, D.A., Baker, H., Dewald, J., Hall, M. and Kallos, G.,** A new class of polymers:Starburst-dendritic macromolecules. *Polymer Journal*, **17**, 117 (1985).

3. **Adam, F., Andas, J. and Rahman, I. A.b**., A facile template-free room temperature synthesis of mesoporouswormlike nickel phyllosilicate. *The Open Colloid Science Journal*, **4**, 12 (2011).

4. **Munshi, S., Dey, G. and Sharma, R. P.**, Use of rice straw ash as pozzolanic material in cement mortar. *IACSIT International Journal of Engineering and Technology*, **5,** 603 (2013).

5. **Ficai, D., Andronescu, E., Ficai, A., Voicu, G. and Vasile, B.,** Synthesis and characterization of mesoporous magnetite based nanoparticles. *Current Nanoscience*, **8**, 875 (2012).

6. *Dendrimers and Other Dendritic Polymers*. Edited by **Jean, M. J. Fre´ chet and Donald A. Tomalia** Copyright © 2001 John Wiley & Sons Ltd ISBNs: 0-471-63850-1(Hardback); 0-470-84582-1 (Electronic).

7. **Lu, T .T., Yang, L .B. and Liaw, W. F.**, *J. Chin. Chem. Soc.* **57**, 909 (2010).

8. **Kurtan,U., Esir, S., Baykal, A. and Sözeri, H.**, *J. Supercond Nov. Magn*. **27**, 2097 (2014).

9. **Wang, B., Wei, Q. and Qu, S**., Synthesis and characterization of uniform and crystalline magnetite nanoparticles via oxidation-precipitation andmodified co-precipitation methods. *Int. J. Electrochem Sci*, **8**, 3786 (2013).

10. **Chou, C.M. and Lien, H.L.,** Dendrimer-conjugated magnetic nanoparticles for removal of zinc (II) from aqueous solutions. *J. Nanopart. Res.*, DOI 10-10071511051-010-9967-5 (2010).

11. **Hassan, S.A. and El-Salamony, R.A.**, Photocatalytic disc-shaped composite systems for removalof hazardous dyes in aqueous solutions. *Canadian Chemical Transition*, **2**, 57 (2014).

(*Received* 4/11/2015;
accepted 11/11/2015)

الخصائص التفاعليه المتحكمة فى تخليق توليفات من جسيمات الحديد المغنطيسى المتشابكه مع دندرايمر البولى أميدو أمين فى وجود رماد قش الأرز

صلاح الدين عبده حسن ، عاطف سمير درويش ، نور الدين أحمد عبد الستار ، هبه محمود جباره* و صفاء رشدى فوده
قسم الكيمياء - كلية العلوم - جامعة عين شمس و*قسم الحفز - شعبة تكرير البترول - معهد بحوث البترول - القاهرة - مصر .

تم فى هذا البحث تحضير توليفة اساسية من جسيمات الماجنيتايت (الحديد المغنطيسى) مع دندرايمر بولى أميدو أمين فى خطوة مباشرة . وقد استتبع ذلك تحضير توليفة مهجنة بإضافة رماد قش الأرز كمادة مالئة وباستخدام نسب مولارية مختلفة من الماجنيتايت متشابكة فى موضعها مع الدندرايمر . تم توصيف هذه التوليفات المجهزة باستخدام تقنيات متطورة مثل XRD, BET, FTIR, DLS, SEM and TEM .

أثبتت الدراسة اشتباك جسيمات الماجنيتايت نانوية الحجم بمجموعات الأمين الأساسية على الجسم التركيبى للدندرايمر وفجواته وذلك من خلال وصلات (N-) O-Fe وذلك فى التوليفة الأم أما فى التوليفة المهجنة فقد ظهر التعامل الحميمى بين رماد قش الأرز عن طريق مجموعاته السيليكيه (Si-OH) ومجموعات الأمين الوظيفية (NH-) بالنهايات الطرفية لسلاسل الدندرايمر وتتراص مكعبات الماجنيتايت نانوية الحجم متشابكة مع جسم الدندرايمر ومطمورة بدرجة تشتت عالية . أما الكربون المتبقى فى تركيب الرماد فقد أعيد توزيعه بدرجة غالبة ليغطى اجزاء كبيره من سطح التوليفة ومالئا لتجويفات الدندرايمر .